




ES-PTAM: Event-based Stereo Parallel Tracking and Mapping

Suman Ghosh^{1,2}, Valentina Cavinato³, and Guillermo Gallego^{1,2,4,5}

¹ Technical University of Berlin, Berlin, Germany

² Robotics Institute Germany, Berlin, Germany

³ Sony Semiconductor Solutions Europe, Sony Europe B.V.,
Stuttgart Laboratory 1, Zürich Office, Switzerland

⁴ Science of Intelligence Excellence Cluster, Berlin, Germany

⁵ Einstein Center Digital Future, Berlin, Germany

Abstract. Visual Odometry (VO) and SLAM are fundamental components for spatial perception in mobile robots. Despite enormous progress in the field, current VO/SLAM systems are limited by their sensors' capability. Event cameras are novel visual sensors that offer advantages to overcome the limitations of standard cameras, enabling robots to expand their operating range to challenging scenarios, such as high-speed motion and high dynamic range illumination. We propose a novel event-based stereo VO system by combining two ideas: a correspondence-free mapping module that estimates depth by maximizing ray density fusion and a tracking module that estimates camera poses by maximizing edge-map alignment. We evaluate the system comprehensively on five real-world datasets, spanning a variety of camera types (manufacturers and spatial resolutions) and scenarios (driving, flying drone, hand-held, egocentric, etc). The quantitative and qualitative results demonstrate that our method outperforms the state of the art in majority of the test sequences by a margin, e.g., trajectory error reduction of 45% on RPG dataset, 61% on DSEC dataset, and 21% on TUM-VIE dataset. To benefit the community and foster research on event-based perception systems, we release the source code and results: <https://github.com/tub-rip/ES-PTAM>.

1 Introduction

Visual odometry (VO) and simultaneous localization and mapping (SLAM) are essential techniques for solving the task of perceiving a robot's location and its 3D environment from visual inputs. This task presents significant challenges, especially in high-speed motion and high dynamic range (HDR) illumination conditions, where conventional cameras may fail due to a common exposure time for all pixels, which limits dynamic range and may produce motion blur. The need for onboard processing in robots with limited computational resources further adds to these challenges [4]. Event cameras are novel bio-inspired sensors that address these challenges by detecting per-pixel brightness changes asynchronously at a high temporal resolution (μs), offering low power consumption, high dynamic range and sparsity for robust and efficient VO/SLAM [11, 13, 23].

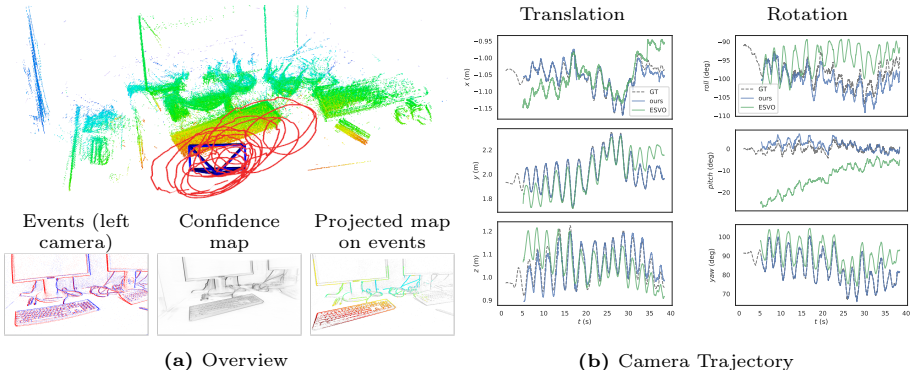


Fig. 1: (a) 3D point cloud and camera trajectory estimated by our stereo VO pipeline for the TUM-VIE *mocap-desk* sequence [21], along with a snapshot of events, confidence map and the projected point cloud (overlaid on the events). Depth is color-coded from red (near) to blue (far away). (b) Estimated camera poses over time, compared to ground truth (GT) and ESVO [37].

Progress in event-based VO/SLAM has been witnessed in monocular [20, 22, 29], and stereo setups [8, 15, 18, 33, 37, 39], possibly aided by other sensors (e.g., depth and/or IMU sensor fusion) [19, 30, 42]. We focus on the stereo case (Fig. 1a), which is particularly suitable for automotive applications, supported by the introduction of new datasets [6, 14, 24, 40], because it can recover the absolute scale of the scene and produces fast depth estimates due to spatial parallax. Moreover, we consider the event-only setting, as our objective is to advance knowledge in purely event-based processing systems, expanding their capabilities while avoiding potential bottlenecks associated with paired sensors [22].

Event-based stereo VO/SLAM methods can be categorized according to multiple criteria (see Tab. 1). Similar to the classification employed for frame-based systems [9], they can be either *feature-based* (indirect) [18, 33] or *direct* [8, 15, 37]. Feature-based methods convert the event data produced by the camera into features (e.g., keypoints), thereby converting the VO/SLAM problem into one based on multi-view geometry. This enables the utilization of classical solutions. Besides compatibility, summarizing the event stream into a few local features also offers speed-up benefits. However, detecting accurate and stable feature tracks poses a challenge due to the dependency of events on motion (unlike conventional images that have motion-invariant properties) and the high amounts of noise (due to the pixels operating at low power). These factors undermine the effectiveness of feature-based VO/SLAM methods. By contrast, direct methods utilize all events recorded by the camera rather than relying solely on those that meet the criteria for a feature. As events are triggered by moving edges, these methods often lead to semi-dense approaches (e.g., involving alignment and/or recovery of edge-like structures).

In this paper, we adopt a direct approach, motivated by the fact that direct methods are state-of-the-art in many event-based motion estimation tasks [17,

Table 1: Stereo event-only VO methods for 6-DOF ego-motion estimation, sorted chronologically. The column D/I indicates whether the method is **D**irect or **I**ndirect (feature-based); the column “Map Prop.” indicates whether local maps are propagated in time and fused or are local only.

Method	D/I	Event representation	Tracking objective	Mapping objective	Map Prop.	Datasets evaluated on
ESVO [37]	D	Time surfaces (TS)	TS as anisotropic distance field	Stereo matching TS patches	✓	RPG, MVSEC, HKUST
Hadviger [18]	I	Arc* corners on TS	Min. reproj. error	Cross-corr. feature descriptors	✗	MVSEC, DSEC
Wang [33]	I	Libviso2 on binary images	Min. reproj. error	Feature matching	✗	MVSEC
El Moudni [8]	D	Raw & Time surfaces (TS)	TS as anisotropic distance field	Ray density fusion	✗	DSEC
Shiba [31]	D	Raw	Max. Contrast	Max. Contrast	✗	DSEC
This work	D	Raw & binary event images	Photometric edge alignment	Ray density fusion	✗	RPG, MVSEC, DSEC TUM-VIE, EVIMO2

26]. Specifically, we improve upon the state-of-the-art mapping method (Multi-Camera Event-based Multi-View Stereo – MC-EMVS) [15], capable of generating semi-dense depth maps from synchronized event cameras. We combine this method with a simple, fast and effective event camera tracker grounded on the idea of (semi-dense) edge-map alignment [29].

In contrast to the pioneering work Event-based Stereo Visual Odometry (ESVO) [37], the MC-EMVS mapper offers several advantages, such as sharper edges, higher accuracy and improved depth map completion [15]. We aim to capitalize on these benefits within a parallel tracking-and-mapping system. Our contributions pertain to system-level aspects, focusing first on designing a coherent system (with compatible mapper and tracker) and then on optimizing performance, thus blending the goals of each module into the central objective of accurate VO. We evaluate our approach on multiple datasets, with different event-camera types, spatial resolutions, calibrations and scene geometries. Table 1 summarizes the theoretical comparison among the state of the art in this topic, as well as the datasets on which the methods have been tested.

As Tab. 1 shows, while MC-EMVS has been used in El Moudni et al. [8], the latter uses different underlying principles for the representations in the tracker and the mapper (time surfaces (TS) vs event counts, respectively), which makes it discordant. The reported results are also limited (only mapping results on a single dataset). Moreover, time surfaces, borrowed from ESVO, define an anisotropic distance field, which results in a biased preference for certain motions. By contrast, our tracker considers an isotropic distance on the image plane, which does not suffer from such a bias. We also characterize overall tracking and mapping performance of the full system with a comprehensive evaluation.

Our work deviates from Zhu et al. [41], which proposes a supervised learning-based system that is trained on stereo data to predict ego-motion and depth, but that at inference time works only on monocular setups. We also differ from Shiba et al. [31], which parameterized the problem using a depth map and optimizes for optical flow, ego-motion and scene depth. Their method only works for short time intervals (where the optical flow is a sensible motion model) and

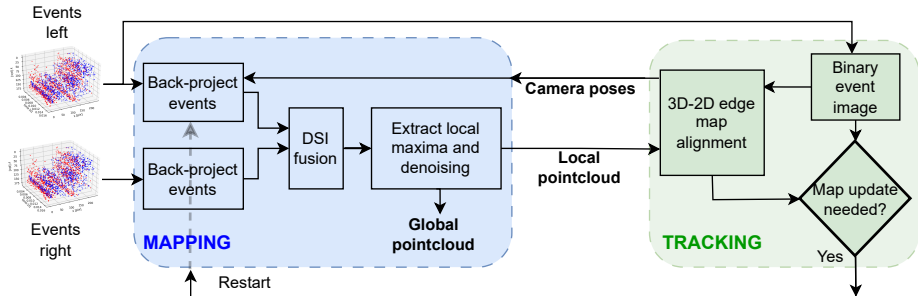


Fig. 2: Proposed event-based stereo visual odometry pipeline consisting of two main modules: camera tracking (i.e., ego-motion estimation) and scene mapping.

provides proof-of-concept results on stereo data. By contrast, our method works on larger (arbitrary) observation intervals, since we do not use the linear motion approximation (optical flow), but rather the full non-linear multi-view equations.

Our main **contributions** can be summarized as follows:

1. A novel event-only stereo VO/SLAM system, which combines an improved version of the MC-EMVS mapper and an edge alignment-based tracker. To the best of our knowledge, it is the first time that this system is proposed.
2. A comprehensive evaluation on *five* datasets, more than any other stereo VO method, outperforming the state of the art in most test sequences.
3. An event-based VO system that naturally scales to multi-camera (≥ 2) setups thanks to the fusion-based architecture of the mapping module. We show, for the first time, results on event-based trinocular VO/SLAM.
4. The source code and results of our stereo system.

2 Methodology

Figure 2 provides an overview of the proposed system. It consists of two main blocks (tracking and mapping modules) operating in parallel (at different rates). Both modules receive events as inputs and rely on each other’s output to maintain proper functionality.

The mapping module is based on MC-EMVS [15], which demonstrated the state-of-the-art depth estimation capabilities when using ground truth (GT) poses. This work proposes additional improvements and demonstrates that the resulting system yields state-of-the-art performance even when pose accuracy is compromised, as shown by its interaction with a simple event camera tracker.

The tracking module is derived from EVO [29], which is grounded on the idea of global image alignment [1]. Whereas the map in EVO [29] is given by EMVS [28], our depth estimates come from a mapping module which extends [28] to multi-camera data fusion via the harmonic mean. The upcoming sections describe each module after briefly reviewing the event camera’s working principle.

2.1 Event Camera Working Principle

Event cameras, such as the Dynamic Vision Sensor (DVS) [23], transmit pixel-wise brightness changes asynchronously, in the form of “events”. An event $e_k \doteq (\mathbf{x}_k, t_k, p_k)$ is produced when the change in log-brightness L reaches a threshold $\theta > 0$:

$$L(\mathbf{x}_k, t_k) - L(\mathbf{x}_k, t_k - \Delta t_k) = p_k \theta, \quad (1)$$

where $\mathbf{x}_k \doteq (x_k, y_k)^\top$, t_k (in μs) and $p_k \in \{+1, -1\}$ are the space-time coordinates and polarity of the event, respectively, and $t_k - \Delta t_k$ is the time of the previous event at the same pixel \mathbf{x}_k . Assuming constant illumination, events are triggered by moving edges on the image plane.

2.2 Stereo Mapping by Ray Density Fusion

Our mapper works on the principle of ray density fusion across stereo cameras [15]. Events are back-projected through 3D space at their corresponding camera location by shooting fictitious rays through 3D space following a space-sweep approach [7]. These give rise to intermediate volumetric representations called Disparity Space Images (DSI), where each point in the volume represents the count of rays that pass through it. Hence, the DSI from each camera reflects the density of viewing rays originating from the events; the higher the density, the higher the likelihood of that point being the location of a 3D edge that triggers the events. The DSIs built from the stereo cameras are then fused into a merged DSI that incorporates the parallax from the stereo configuration and balances the events triggered at each camera. This fused DSI is then used to extract depth information (candidate locations of 3D edges) by local maxima detection.

Formally, let $\mathcal{E}_l = \{e_k^l\}_{k=1}^{N_l^e}$ ($l \equiv \text{left}$) and $\mathcal{E}_r = \{e_k^r\}_{k=1}^{N_r^e}$ ($r \equiv \text{right}$) be stereo events over some time interval $[0, T]$, and $f_l, f_r : V \subset \mathbb{R}^3 \rightarrow \mathbb{R}_{\geq 0}$ be the corresponding ray densities (DSIs) defined over a volume V . That is,

$$f_l(\mathbf{X}) = \sum_{k=1}^{N_l^e} \delta(\mathbf{X} - \mathbf{X}'_k(e_k^l)), \quad (2)$$

where $\mathbf{X}'_k(e_k^l) = (\mathbf{x}_k^{l\top}, Z)^\top$ is a 3D point on the back-projected ray through event e_k^l , at depth Z with respect to a reference view (RV). Events are transferred to RV using a warp \mathbf{W} defined by the continuous motion of the cameras and candidate space-sweep depth values $Z \in [Z_{\min}, Z_{\max}]$, $\mathbf{x}_k^{l\prime} = \mathbf{W}(e_k^l, \mathbf{P}^l(t_k), \mathbf{P}_v, Z)$, where $\mathbf{P}^l(t)$ is the pose of the left event camera at time t and \mathbf{P}_v is the pose of RV. In implementation, DSIs are discretized over a projective voxel grid with N_Z depth planes, and the Delta δ in (2) is approximated by bilinear voting [28]. Hence, each voxel counts the number of event-viewing rays that pass through it.

Among the multiple fusion schemes available in MC-EMVS we choose a point-wise (i.e., voxel-wise) harmonic mean fusion across cameras and no extra fusion in time due to its high accuracy and speed [15]. Specifically, if $f_l(\mathbf{X}), f_r(\mathbf{X})$ are the DSI values at a 3D point \mathbf{X} , the fused DSI value at that point is given by

$$f_{\text{stereo}}(\mathbf{X}) = 2 / (1/f_l(\mathbf{X}) + 1/f_r(\mathbf{X})). \quad (3)$$

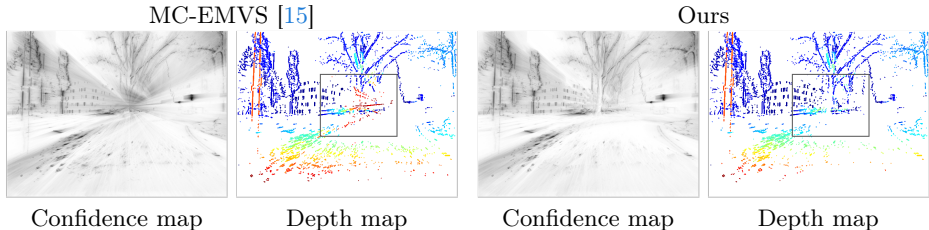


Fig. 3: Our improved ray casting produces clean confidence and depth maps. See its effect near the focus of expansion. Depth is color-coded from red (near) to blue (far).

The output depth Z^* at each pixel of the RV is obtained from the fused DSI as the local maxima after applying adaptive Gaussian thresholding and a median filter for denoising. This approach has connections with Contrast Maximization [12]. The maximum of the DSI at each of its viewing pixels allows us to compute the “confidence map” (Fig. 1a); the higher its value the more rays intersect from both cameras, providing more evidence for the presence of scene edges (note that Fig. 1a is in negated form: dark indicating high confidence). Finally, the depth map is converted into a point cloud (local 3D map \mathcal{M} at RV).

Improvements with respect to MC-EMVS [15]. The mapper processes events in batches of fixed number of events N_e (instead of a constant time window [15]). This adapts better to the amount of motion in the scene assuming that the texture is approximately constant. Also, for improved robustness to noise, we set a minimum and maximum limit for the duration spanned by N_e events, to deal with cases with too high event rate (e.g., flashing lights) or too low event rate (e.g., ambient noise while stationary).

Additionally, we propose a new event back-projection strategy to deal with scenarios where the camera trajectory lies within the 3D volume spanned by the current DSI. This happens, for instance, when the camera moves along its optical axis, in the forward or backward direction. In such scenarios, a pathologically high ray density is produced in the DSI due to the fact that the rays emanate from points inside the DSI (i.e., the optical centers of the camera poses). The optical centers of other camera locations seen from the reference view (RV) thus erroneously appear as highly confident 3D point estimates. This happens because all the rays that cast from a camera also seem to intersect at its own optical center. MC-EMVS [15] circumvented this issue by always setting the DSI RV at the end of the camera trajectory in forward moving scenes, but this strategy does not work for arbitrary motions (e.g., moving backwards). Here, we provide a general solution to the problem for all kinds of motion by limiting the ray casting to depth planes beyond Z_{\min} distance from the optical center in the forward direction.

Figure 3 compares the proposed strategy to that in MC-EMVS [15] on a section of the DSEC driving dataset [14], showing a clear improvement. This

modification allows us to unlock 3D mapping even during forward and backward motion along the camera’s optical axis, which is necessary for robust 6-DOF VO.

2.3 Camera Tracking by Edge-Map Alignment

Our system tracks the motion of the stereo rig using only one of the cameras (“Left” in Fig. 2). This approach is chosen because tracking using more than one camera does not offer significant advantages, but it introduces additional computational cost (see [37]).

Since we aim to demonstrate the effectiveness of the fusion-based mapping module for visual odometry, we use an event-based camera tracker that works on the produced semi-dense 3D maps, by leveraging the idea of edge-map alignment [29]. This tracker operates by minimizing (in the Lie group of rigid body motions $SE(3)$) a simplified photometric error between two bimodal images. Specifically,

$$\min_{T \in SE(3)} \sum_{\mathbf{p}} (E(\mathbf{p}; T, \mathcal{M}) - B(\mathbf{p}))^2. \quad (4)$$

One image is an edge map E obtained by projecting the current semi-dense 3D map (point cloud) \mathcal{M} onto the camera’s image plane at a candidate pose $T \in SE(3)$. The other image is formed by event counting: as the camera moves, a small number of events are accumulated into a binary image B (pixels where events have been triggered are marked as ‘1’ over a ‘0’ canvas). If the number of events is small, there is no motion blur in the accumulated image, i.e., it forms a sharp edge map that resembles the projected point cloud. Consequently, we estimate the incremental pose necessary to align the projected map with the event image by minimizing their “intensity” error (4) (sampled at a subset of the pixels, for speed-up). The minimization is achieved using the inverse compositional Lucas-Kanade algorithm [1]. To aid the optimizer, smoothness in the error function is introduced by applying a Gaussian blur to the projected map.

2.4 Module Interaction: Parallel Tracking and Mapping

The mapping and tracking modules described in the previous sections operate in parallel, communicating (Fig. 2) via ROS [27]. Both modules operate asynchronously in an event-driven manner. During motion, camera poses are progressively estimated (every M events) by the tracker (by composing incremental poses) as long as there is sufficient overlap in the field of view (FOV) between the already estimated 3D maps and the current camera view. When the camera moves into an unobserved part of the scene that has not yet been mapped or when the motion parallax is above a threshold, a new map update is requested using all the estimated poses and the most recent N_e events from both cameras.

In addition to the above “on-demand” mode of operation (FOV overlap), it is also possible to operate the mapper at a fixed rate. Since the mapping process is computationally more expensive than the tracking operation, it is done at a considerably slower rate (e.g., 5 maps/s vs. 50–150 poses/s). It is advisable to run the mapper in “on-demand” mode for scenarios with large event rates

Table 2: Absolute Trajectory Error (ATE) and Absolute Rotation Error [34] (ARE) on datasets of multiple resolutions (and therefore varying event rates). All the values for EVO [29] are taken from [22]. ESVO values are taken from the authors’ latest paper [25], except for the TUM-VIE dataset on which we re-ran ESVO [37]. Rotation errors on the RPG dataset were taken from [22]. (-) indicates missing values. (*) indicates failure in after completing at most 30% of the sequence. (†) indicates when the first 6s were skipped because of large independent motion in the system’s FOV.

Dataset	Seq.	Time [s]	Length [cm]	#Ev./cam [million]	ATE RMSE [cm]			ARE RMSE [deg]		
					EVO	ESVO	Ours	EVO	ESVO	Ours
RPG [36] (240×180 px)	monitor	23	675	13	7.8	5.8	2.34	7.77	2.74	1.52
	desk	13	403	9	5.2	7.25	2.84	8.25	7.25	3.44
	bin	17	514	9	13.2*	-	2.57	50.26*	7.61	3.29
	boxes	15	704	12	14.2*	9.5	4.06	170.36*	9.46	6.62
DSEC [14] (640×480 px)	zc04a	35.0	23172	359	-	371.1	131.62	-	-	3.17
	zc04b	13.4	5888	130	-	116.6	29.02	-	-	2.04
	zc04c	59.0	52465	391	-	1357.1	1184.37†	-	-	6.02†
	zc04d	47.8	53994	325	-	2676.6	1053.87	-	-	37.13
	zc04e	13.6	12278	119	-	794.9	75.9	-	-	3.97
	zc04f	43.1	38758	362	-	-	522	-	-	10.65
TUM-VIE [21] (1280×720 px)	1d-trans	36.6	502	573	7.5	12.31	1.05	-	7.77	6.02
	3d-trans	33.2	719	871	12.5	17.17	8.53	-	33.67	15.62
	6dof	19.5	531	568	85.5	13.04	10.25	-	10.76	14.01
	desk	37.5	1033	1130	54.1	12.38	2.5	-	17.48	3.37
	desk2	21.4	568	643	75.2	4.56	7.2	-	5.09	10.12

like with high-speed motion or high camera resolution. In practice, for efficiency and memory optimization, we retain only a single local map for pose estimation, which has proven to be sufficient for proper operation. Local maps are aggregated into a global point cloud for visualization.

There are several ways in which the system can be initialized / bootstrapped, depending on the specific event camera used. One possibility is, as in [29], initialization by classical epipolar-geometry methods on event images. Some devices, like the DAVIS [32], concurrently output events, grayscale frames and IMU data. In such cases, initial poses may be obtained from running a frame-based method (e.g., SVO [10]) on the DAVIS frames, by IMU dead-reckoning or by a VIO method (e.g., EVIO [38], ROVIO [2]).

The mapping operation is automatically started after an initial wait period (typically 0.5s) using poses from any of the above bootstrapping methods. Once an initial map is available, tracking also starts automatically. From this point onwards, the estimated camera poses produced by our event-based tracker are used for subsequent mapping.

3 Experiments

3.1 Datasets and Metrics

We evaluate the performance of our stereo VO pipeline on sequences from *five* publicly available datasets [3, 14, 21, 36, 40] with varying camera resolutions depicting a wide range of scenarios on different mobile platforms. Most of the

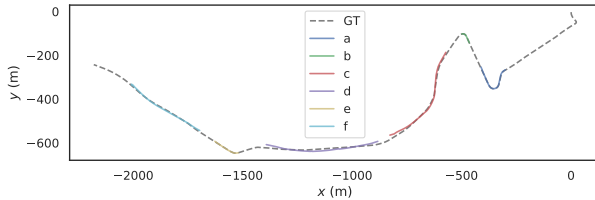


Fig. 4: Estimated trajectory of *zurich_city_04* sequence from the DSEC dataset vs ground truth. The six evaluation segments (a)-(f) correspond to the rows of Tab. 2.

datasets contain ground truth (GT) poses from a motion capture (mocap) system. Where camera poses are not available, like in DSEC [14], we use LiDAR-inertial odometry data provided by the authors as ground truth. We use ground truth poses for accuracy assessment and also for bootstrapping.

Qualitative evaluation of our VO pipeline is done by visualizing the estimated camera trajectories and 6-DOF (degrees of freedom) pose, and comparing it to ground truth (using [16]), along with depth maps and point clouds.

Similar to recent event-based VO methods in the literature [22,25,37], we perform quantitative evaluation by computing the root-mean-square (RMSE) Absolute Trajectory Errors (ATE) and Absolute Rotation Errors (ARE) on tracked camera poses using the tool in [34] (Tab. 2). These combine the effects of both mapping and tracking estimation errors into a single metric. This is because map errors leak into trajectory errors and vice-versa cumulatively, and trajectory errors are easier to assess than mapping errors. Additionally, we carry out a broad evaluation of the performance of the improved mapper (Fig. 3) using ten standard quantitative metrics in Sec. 3.3.

In this work, we compare the camera tracking performance of our system with the state-of-the-art direct event-only stereo visual odometry method ESVO [37] and with monocular system EVO [29]. Table 2 provides a comprehensive comparison of these methods on standard datasets of different resolutions.

It was not possible to compare to other methods in Tab. 1 because code was unavailable [8, 18, 33] and/or trajectory errors were either not reported [8], or did not use the same standard metrics as in ESVO (e.g., absolute errors) [18].

Since our system is intended for live operation, experiments were performed in an online manner by playing ROSBags (slowed down for high resolution cameras), launching our tracking and mapping nodes, and recording the output poses and point clouds in real-time. Results may vary slightly depending on the CPU load, ROSBag playback speed and available processing power (as in ESVO).

3.2 Results

RPG Stereo Dataset. This dataset was recorded with stereo DAVIS cameras with 240×180 px resolution mounted on a handheld rig [36]. It comprises various indoor scenes inside a mocap room with 6-DOF camera motion. Table 2 lists ATE and ARE for camera poses estimated by EVO, ESVO and our system on some

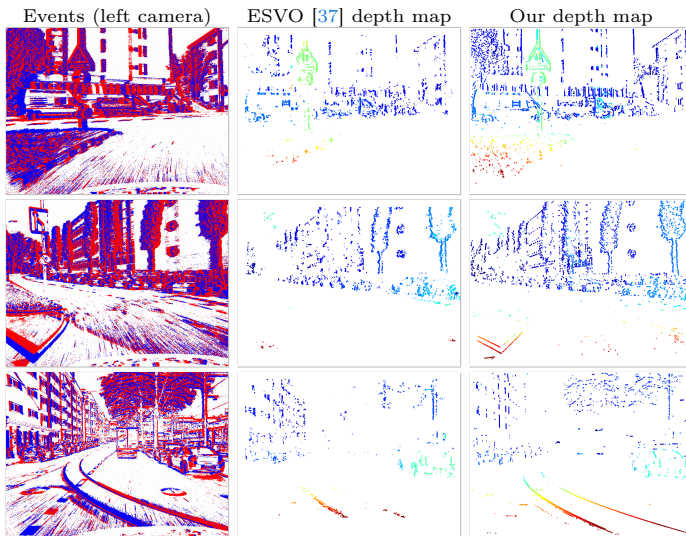


Fig. 5: Results on DSEC using our method and ESVO. The sharper edge maps from our method allow us to track camera poses accurately using edge alignment.

commonly used sequences of this dataset. For this dataset, we found different ATE values reported for ESVO in different papers, which may be due to its non-deterministic nature. Here, we report the values from the latest work by the same authors [25]. Since ARE is missing from that paper, we take them from [22]. We observe that our system performed best, while EVO failed after completing at most 30% of the *bin* and *boxes* sequences.

DSEC Driving Dataset. The sequences in the DSEC dataset [14] were recorded with VGA resolution (640×480 px) stereo event cameras on a car driven through the streets of Switzerland. Driving scenarios are challenging for event-based sensors because forward motions typically produce considerably fewer events in the center of the image (where apparent motion is small) than in the periphery. Forward motion is also particularly challenging for 3D reconstruction compared to sideways motions due to lack of motion parallax. For the evaluation, we used the *zurich_city_04* sequences that contain many flashing lights (from vehicles and street signs) and Independently Moving Objects (IMOs), which makes it challenging for event-based motion estimation.

Figure 4 shows small drift of the estimated trajectory of the car-mounted camera on all parts of the ≈ 2 km drive, whereas Tab. 2 reports that, compared to ESVO, our system is more accurate (in some cases by an order of magnitude). This is mainly due to better depth estimation performance of the ray density fusion-based mapping module compared to ESVO, as demonstrated in [8, 15], and further illustrated in Fig. 5 where we are able to reconstruct denser and sharper 3D edge maps that preserve details, even without map propagation.

The first 6s of the *zurich_city_04_c* sequence comprises a tram moving very close to the car and occupying majority of the cameras’ FOV. The scene is dominated by events generated from independent motion, and our assumption of a static world becomes invalid, causing tracking failure. We thus report results after 6s, when the tram has moved sufficiently far away. It should be noted that the ESVO tracker also fails during this phase but thanks to its re-initialization module, it can recover and complete the sequence.

TUM-VIE Dataset. This dataset was recorded with stereo HD (1 Megapixel) event cameras mounted on a helmet and recorded from an egocentric viewpoint [21]. We report results on sequences recorded in a mocap room containing varying DOFs of camera motion, spanning two distinct sets of calibration parameters. We also re-ran ESVO in this case.

A major issue in the mocap sequences is the large amount of noisy events generated by flashing (IR or LED) lights throughout the sequence. Particularly, the first few seconds of each sequence contain flashing fluorescent lights without any camera motion. We thus start both ESVO and our pipeline after the flashes subside (typically after 5s). Moreover, the scene depth in these sequences is small relative to the camera baseline (11.84 cm). If we set the reference view of our map on one camera trajectory, the large baseline makes the event rays back-projected from the other camera appear nearly parallel in the DSI, which hampers sharpening of edges during fusion.

Despite these challenges, Tab. 2 shows that we obtain better ATE in all but one sequence, and better ARE in 60% of the evaluated sequences. We also show qualitative results on the longest sequence *desk*. Figure 1 depicts the estimated global point cloud and camera trajectory for the full 33s sequence (with over 1 *billion* events), along with snapshots of the events, the confidence map and the projected local point cloud. The camera performs multiple loops with 6-DOF motion in this sequence. Even without any back-end or map fusion through time, the resulting point cloud preserves details and sharp edges, showcasing minimal drift in our system. Figure 1b further compares the 6-DOF pose estimates over time against the ground truth and ESVO; the latter shows considerable drift in both translation and rotation.

Compared to EVO, our stereo VO pipeline produces more accurate results because it not only leverages temporal stereo, but also spatial parallax. This is especially noticeable in some of the sequences, like *desk*, with an ATE improvement from 54.1 cm to 2.5 cm (Tab. 2). Such improvement is also observed for the RPG dataset (see the top part of Tab. 2).

EVIMO2 Trinocular Dataset. Adding more than two cameras to a sensor setup can improve 3D reconstruction by better handling occlusions and removing ambiguities [5]. Most stereo methods estimate depth by matching features across image pairs. For N cameras, this involves a combinatorial number of matching steps, ${}^N C_2$ times (3 times for 3 cameras, 12 times for 4 cameras, etc.). This makes multi-camera stereo prohibitively expensive for real-time SLAM/VO despite the

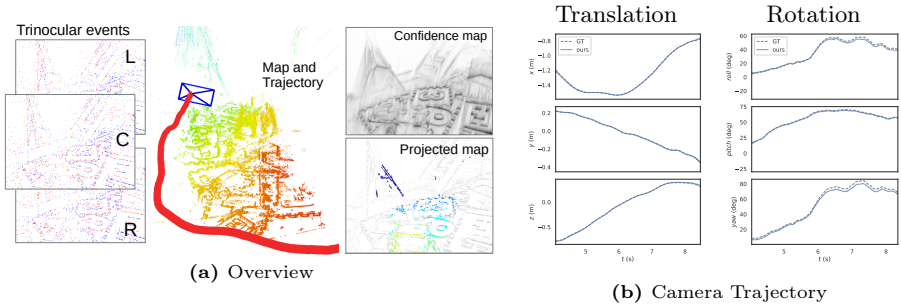


Fig. 6: Results on trinocular camera dataset EVIMO2. (a) Sensor rig trajectory, point cloud and depth map from our proposed VO system on *scene_03_00_000000* SFM sequence). The point cloud is color-coded from red (near) to blue (far away). (b) Degrees of freedom (DOFs) of estimated poses compared to ground truth poses.

promised benefits. By foregoing the need for finding pairwise correspondences, our mapping module scales with linear complexity – for N cameras, the DSI creation and fusion steps are done N times (see [15]). Our system thus unlocks the use of multi-camera setups for event-based VO/SLAM for the first time.

We present results on the only existing trinocular event dataset EVIMO2 [3], recorded using a handheld rig with three VGA resolution event cameras in an indoor environment. Unfortunately, there is narrow overlap between the FOVs of the cameras because the Prophesee Gen3 cameras on either side are in portrait mode, whereas the Samsung DVS, in the center, is in landscape mode. This makes depth estimation difficult when the cameras approach too close to the objects placed on a table, as they may fall outside the overlapping FOV. We set the central camera as the reference for both tracking and mapping.

Figure 6 shows the camera trajectory and global semi-dense point cloud estimated by our VO system as it goes around a table top. The system exhibits very good tracking accuracy when there is sufficient overlap among the camera views. For comparison, we also tried a stereo configuration with just the left and right event cameras, but the VO system lost track easily due to the smaller overlap between the cameras (compared to the trinocular configuration). This experiment exemplifies the benefit of having redundancy in the trinocular system.

MVSEC Dataset. Finally, we also present results on the MVSEC dataset [40]. The low spatial resolution (346×260 px), small baseline of the stereo rig and few events generated far from the camera are challenging factors for accurate pose estimation. The outdoor sequences are not usable in stereo since the baseline is too small [15] compared to a 1-pixel disparity resolution.

We thus show qualitative results on the *indoor_flying1* sequence, which comprises arbitrary 6-DOF motion from a camera-mounted drone flying inside a mop-cap room. The quick forward and backward motion of the drone combined with hovering halts (with almost no events generated) in between make it especially

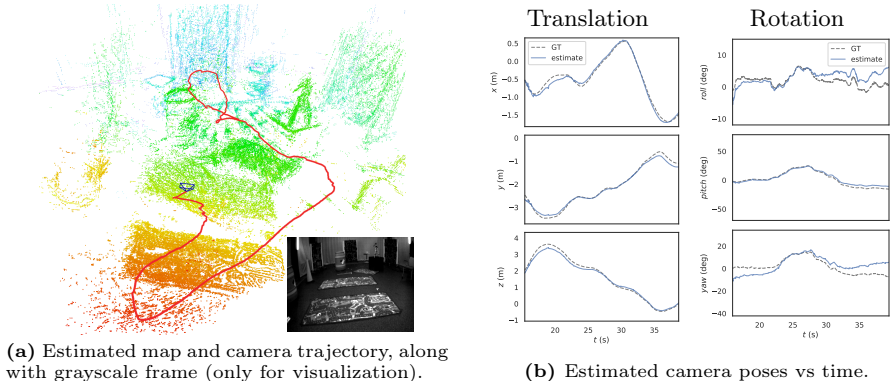


Fig. 7: Results on MVSEC *indoor_flying1* sequence.

Table 3: Evaluation of depth estimation on DSEC with a maximum range of 50 m. All methods use GT poses from LiDAR-inertial odometry. The methods are evaluated on 35s of stereo data, consisting of 635 million events and containing 350 GT depth maps. Each depth map is computed using 1 s of event data (≈ 10 million events). ESVO is executed fusing 10 depth maps generated at 10 Hz (LiDAR rate), i.e., 1 s of event data.

Algorithm	Mean Err [m] ↓	Median Err [m] ↓	bad-pix [%] ↓	SILog Err $\times 100$ ↓	AErRr [%] ↓	log RMSE $\times 100$ ↓	$\delta < 1.25$ [%] ↑	$\delta < 1.25^2$ [%] ↑	$\delta < 1.25^3$ [%] ↑	#Points [million] ↑
EMVS [28] (monocular)	5.17	0.99	13.96	33.68	59.92	59.97	82.77	87.41	89.15	1.62
ESVO [37]	3.93	1.62	10.54	8.30	17.66	28.90	84.37	92.81	96.05	9.40
MC-EMVS [15]	3.13	0.66	7.68	14.07	24.56	37.85	90.37	93.28	94.84	2.38
Limit rays on MC-EMVS	2.90	0.68	5.97	6.52	11.60	25.55	91.54	94.85	96.56	2.31

challenging. The drone also often comes very close to the reflective and salt-and-pepper textured ground surface, which generates many unstructured brightness changes, further challenging event-based VO.

Nevertheless, our system successfully tracks long stretches of the flight involving to-fro motion, sudden change of direction, hoverings and loops, as shown in Fig. 7, which depicts the estimated trajectory and global point cloud, and the individual camera DoFs compared with ground truth. While our system estimates translations accurately, we observe small accumulation of drift in the orientation.

3.3 Depth Estimation Ablation

The results of depth estimation of our mapper on the full DSEC *zurich04a* driving sequence are reported in Tab. 3. We followed the evaluation protocol in [15], as detailed in the caption. For MC-EMVS and EMVS, the DSI reference views were set at the camera trajectory center. The last row corresponds to our improved MC-EMVS (Sec. 2.2), where the reprojected rays are limited to a minimum depth plane, making it robust to all forward and backward motions. With this change, camera centers are not mistaken for 3D structures (see Fig. 3), significantly improving depth estimation accuracy (32.5% drop in log-RMSE).

Table 4: Runtime of different steps of our stereo method processing DAVIS346 data.

Module	Function (Parameters)	Time [ms]
Mapper	DSI creation (2M events per camera, 100 depth planes)	45
	DSI fusion (two DSIs)	26
	arg max	21
	Adaptive Gaussian Thresholding (5×5 px kernel)	0.2
Tracker	Event map creation (10k events)	0.4
	Optimization (1k batch size, 2 pyramid levels, 150 max iterations)	6–20

3.4 Computational Performance

Tests were run on a desktop computer with CPUs of Intel Xeon(R) W-2225 at 4.10GHz×8 cores. The runtime numbers for processing MVSEC data (stereo DAVIS346 cameras with 346×260 px resolution) are reported in Tab. 4. As observed, the slowest component of the system is the DSI creation in the mapper. This processing time can be reduced by decreasing the number of depth planes (at the expense of some loss of precision in depth) or by parallelizing using GPUs. Nevertheless, this is not always needed: in the accompanying video, we demonstrate live operation of our system with a stereo DAVIS346 setup.

3.5 Limitations

While the parallel-tracking-and-mapping strategy works and is common to many approaches, the propagation of errors, and therefore the growth of drift is inevitable. This could be mitigated by incorporating a refinement step (bundle adjustment) in the system. This is an emerging avenue for future research [17].

Furthermore, most SLAM methods lack a strategy to exclude such large distractors (IMOs), which can cause drift (as observed in the experiments). Dealing with them, possibly via a combination with motion segmentation [35], is still an unexplored topic in the incipient field of event-based SLAM.

4 Conclusion

We have introduced a novel event-only stereo visual odometry system. It has a geometric design, combining a mapping module based on the idea of ray density fusion, with improved capabilities over MC-EMVS, and a tracking module based on the idea of global edge-map alignment. The proposed method has been thoroughly tested on five datasets, more than any of the previous works, and it outperforms the state-of-the-art ESVO and EVO methods by a margin. The experiments show the remarkable capabilities of our method to handle a wide range of scenes, event camera types and spatial resolutions (from HQVGA to HD), outputting accurate camera trajectories and sharp semi-dense maps. Future exciting research directions for improvement comprise large IMO handling and a back-end refinement. We release the source code and hope that our work fosters research into event-based VO methods for autonomous vehicles and robots.

Acknowledgments

Funded by the SONY Research Award Program 2021. Funded by the Deutsche Forschungsgemeinschaft (DFG, German Research Foundation) under Germany's Excellence Strategy – EXC 2002/1 “Science of Intelligence” – project number 390523135.

References

1. Baker, S., Matthews, I.: Lucas-kanade 20 years on: A unifying framework. *Int. J. Comput. Vis.* **56**(3), 221–255 (2004). <https://doi.org/10.1023/B:VISI.0000011205.11775.fd>
2. Bloesch, M., Omari, S., Hutter, M., Siegwart, R.: Robust visual inertial odometry using a direct EKF-based approach. In: *IEEE/RSJ Int. Conf. Intell. Robot. Syst. (IROS)*. pp. 298–304 (2015). <https://doi.org/10.1109/IROS.2015.7353389>
3. Burner, L., Mitrokhin, A., Fermüller, C., Aloimonos, Y.: EVIMO2: An event camera dataset for motion segmentation, optical flow, structure from motion, and visual inertial odometry in indoor scenes with monocular or stereo algorithms. *arXiv e-prints* (May 2022). <https://doi.org/10.48550/arXiv.2205.03467>
4. Cadena, C., Carlone, L., Carrillo, H., Latif, Y., Scaramuzza, D., Neira, J., Reid, I.D., Leonard, J.J.: Past, present, and future of simultaneous localization and mapping: Toward the robust-perception age. *IEEE Trans. Robot.* **32**(6), 1309–1332 (2016). <https://doi.org/10.1109/TRO.2016.2624754>
5. Carneiro, J., Ieng, S.H., Posch, C., Benosman, R.: Event-based 3D reconstruction from neuromorphic retinas. *Neural Netw.* **45**, 27–38 (2013). <https://doi.org/10.1016/j.neunet.2013.03.006>
6. Chaney, K., Cladera Ojeda, F., Wang, Z., Bisulco, A., Hsieh, M.A., Korpela, C., Kumar, V., Taylor, C.J., Daniilidis, K.: M3ED: Multi-robot, multi-sensor, multi-environment event dataset. In: *IEEE Conf. Comput. Vis. Pattern Recog. Workshops (CVPRW)*. pp. 4016–4023 (2023). <https://doi.org/10.1109/CVPRW59228.2023.00419>
7. Collins, R.T.: A space-sweep approach to true multi-image matching. In: *IEEE Conf. Comput. Vis. Pattern Recog. (CVPR)*. pp. 358–363 (1996). <https://doi.org/10.1109/CVPR.1996.517097>
8. El Moudni, A., Morbidi, F., Kramm, S., Boutteau, R.: An event-based stereo 3D mapping and tracking pipeline for autonomous vehicles. In: *IEEE Intell. Transp. Sys. Conf. (ITSC)*. pp. 5962–5968 (2023). <https://doi.org/10.1109/ITSC57777.2023.10422404>
9. Engel, J., Koltun, V., Cremers, D.: Direct Sparse Odometry. *IEEE Trans. Pattern Anal. Mach. Intell.* **40**(3), 611–625 (Mar 2018). <https://doi.org/10.1109/TPAMI.2017.2658577>
10. Forster, C., Zhang, Z., Gassner, M., Werlberger, M., Scaramuzza, D.: SVO: Semidirect visual odometry for monocular and multicamera systems. *IEEE Trans. Robot.* **33**(2), 249–265 (2017). <https://doi.org/10.1109/TRO.2016.2623335>
11. Gallego, G., Delbruck, T., Orchard, G., Bartolozzi, C., Taba, B., Censi, A., Leutenegger, S., Davison, A., Conradt, J., Daniilidis, K., Scaramuzza, D.: Event-based vision: A survey. *IEEE Trans. Pattern Anal. Mach. Intell.* **44**(1), 154–180 (2022). <https://doi.org/10.1109/TPAMI.2020.3008413>

12. Gallego, G., Rebecq, H., Scaramuzza, D.: A unifying contrast maximization framework for event cameras, with applications to motion, depth, and optical flow estimation. In: IEEE Conf. Comput. Vis. Pattern Recog. (CVPR). pp. 3867–3876 (2018). <https://doi.org/10.1109/CVPR.2018.00407>
13. Gehrig, D., Scaramuzza, D.: Low-latency automotive vision with event cameras. *Nature* **629**(8014), 1034–1040 (2024). <https://doi.org/10.1038/s41586-024-07409-w>
14. Gehrig, M., Aarents, W., Gehrig, D., Scaramuzza, D.: DSEC: A stereo event camera dataset for driving scenarios. *IEEE Robot. Autom. Lett.* **6**(3), 4947–4954 (2021). <https://doi.org/10.1109/LRA.2021.3068942>
15. Ghosh, S., Gallego, G.: Multi-event-camera depth estimation and outlier rejection by refocused events fusion. *Adv. Intell. Syst.* **4**(12), 2200221 (2022). <https://doi.org/10.1002/aisy.202200221>
16. Grupp, M.: evo: Python package for the evaluation of odometry and slam. <https://github.com/MichaelGrupp/evo> (2017)
17. Guo, S., Gallego, G.: CMax-SLAM: Event-based rotational-motion bundle adjustment and SLAM system using contrast maximization. *IEEE Trans. Robot.* **40**, 2442–2461 (2024). <https://doi.org/10.1109/TRO.2024.3378443>
18. Hadviger, A., Cvišić, I., Marković, I., Vražić, S., Petrović, I.: Feature-based event stereo visual odometry. In: Eur. Conf. Mobile Robots (ECMR). pp. 1–6 (2021). <https://doi.org/10.1109/ECMR50962.2021.9568811>
19. Hidalgo-Carrió, J., Gallego, G., Scaramuzza, D.: Event-aided direct sparse odometry. In: IEEE Conf. Comput. Vis. Pattern Recog. (CVPR). pp. 5781–5790 (Jun 2022). <https://doi.org/10.1109/CVPR52688.2022.00569>
20. Kim, H., Leutenegger, S., Davison, A.J.: Real-time 3D reconstruction and 6-DoF tracking with an event camera. In: Eur. Conf. Comput. Vis. (ECCV). pp. 349–364 (2016). https://doi.org/10.1007/978-3-319-46466-4_21
21. Klenk, S., Chui, J., Demmel, N., Cremers, D.: TUM-VIE: The TUM stereo visual-inertial event dataset. In: IEEE/RSJ Int. Conf. Intell. Robot. Syst. (IROS). pp. 8601–8608 (2021). <https://doi.org/10.1109/IROS51168.2021.9636728>
22. Klenk, S., Motzet, M., Koestler, L., Cremers, D.: Deep event visual odometry. In: Int. Conf. 3D Vision (3DV). pp. 739–749 (2024). <https://doi.org/10.1109/3DV62453.2024.00036>
23. Lichtsteiner, P., Posch, C., Delbruck, T.: A 128×128 120 dB 15 μ s latency asynchronous temporal contrast vision sensor. *IEEE J. Solid-State Circuits* **43**(2), 566–576 (2008). <https://doi.org/10.1109/JSSC.2007.914337>
24. Mollica, G., Felicioni, S., Legittimo, M., Meli, L., Costante, G., Valigi, P.: MAVIED: A multisensor automotive visual inertial event dataset. *IEEE Trans. Intell. Transport. Syst.* **25**(1), 214–224 (2024). <https://doi.org/10.1109/TITS.2023.3312355>
25. Niu, J., Zhong, S., Zhou, Y.: IMU-aided event-based stereo visual odometry. In: IEEE Int. Conf. Robot. Autom. (ICRA). pp. 11977–11983 (2024). <https://doi.org/10.1109/ICRA57147.2024.10611439>
26. Nunes, U.M., Demiris, Y.: Robust event-based vision model estimation by dispersion minimisation. *IEEE Trans. Pattern Anal. Mach. Intell.* **44**(12), 9561–9573 (2022). <https://doi.org/10.1109/TPAMI.2021.3130049>
27. Quigley, M., Conley, K., Gerkey, B., Faust, J., Foote, T., Leibs, J., Wheeler, R., Ng, A.Y.: ROS: an open-source Robot Operating System. In: ICRA Workshop Open Source Softw. pp. 1–5 (2009)

28. Rebecq, H., Gallego, G., Mueggler, E., Scaramuzza, D.: EMVS: Event-based multi-view stereo—3D reconstruction with an event camera in real-time. *Int. J. Comput. Vis.* **126**(12), 1394–1414 (Dec 2018). <https://doi.org/10.1007/s11263-017-1050-6>
29. Rebecq, H., Horstschäfer, T., Gallego, G., Scaramuzza, D.: EVO: A geometric approach to event-based 6-DOF parallel tracking and mapping in real-time. *IEEE Robot. Autom. Lett.* **2**(2), 593–600 (2017). <https://doi.org/10.1109/LRA.2016.2645143>
30. Rosinol Vidal, A., Rebecq, H., Horstschaefer, T., Scaramuzza, D.: Ultimate SLAM? combining events, images, and IMU for robust visual SLAM in HDR and high speed scenarios. *IEEE Robot. Autom. Lett.* **3**(2), 994–1001 (Apr 2018). <https://doi.org/10.1109/LRA.2018.2793357>
31. Shiba, S., Klose, Y., Aoki, Y., Gallego, G.: Secrets of event-based optical flow, depth, and ego-motion by contrast maximization. *IEEE Trans. Pattern Anal. Mach. Intell.* pp. 1–18 (2024). <https://doi.org/10.1109/TPAMI.2024.3396116>
32. Taverni, G., Moeys, D.P., Li, C., Cavaco, C., Motsnyi, V., Bello, D.S.S., Delbruck, T.: Front and back illuminated Dynamic and Active Pixel Vision Sensors comparison. *IEEE Trans. Circuits Syst. II (TCSII)* **65**(5), 677–681 (2018). <https://doi.org/10.1109/TCSII.2018.2824899>
33. Wang, J., Gammell, J.D.: Event-based stereo visual odometry with native temporal resolution via continuous-time Gaussian process regression. *IEEE Robot. Autom. Lett.* **8**(10), 6707–6714 (2023). <https://doi.org/10.1109/LRA.2023.3311374>
34. Zhang, Z., Scaramuzza, D.: A tutorial on quantitative trajectory evaluation for visual(-inertial) odometry. In: *IEEE/RSJ Int. Conf. Intell. Robot. Syst. (IROS)*. pp. 7244–7251 (2018). <https://doi.org/10.1109/IROS.2018.8593941>
35. Zhou, Y., Gallego, G., Lu, X., Liu, S., Shen, S.: Event-based motion segmentation with spatio-temporal graph cuts. *IEEE Trans. Neural Netw. Learn. Syst.* pp. 1–13 (2021). <https://doi.org/10.1109/TNNLS.2021.3124580>
36. Zhou, Y., Gallego, G., Rebecq, H., Kneip, L., Li, H., Scaramuzza, D.: Semi-dense 3D reconstruction with a stereo event camera. In: *Eur. Conf. Comput. Vis. (ECCV)*. pp. 242–258 (2018). https://doi.org/10.1007/978-3-030-01246-5_15
37. Zhou, Y., Gallego, G., Shen, S.: Event-based stereo visual odometry. *IEEE Trans. Robot.* **37**(5), 1433–1450 (2021). <https://doi.org/10.1109/TRO.2021.3062252>
38. Zhu, A.Z., Atanasov, N., Daniilidis, K.: Event-based visual inertial odometry. In: *IEEE Conf. Comput. Vis. Pattern Recog. (CVPR)*. pp. 5816–5824 (2017). <https://doi.org/10.1109/CVPR.2017.616>
39. Zhu, A.Z., Chen, Y., Daniilidis, K.: Realtime time synchronized event-based stereo. In: *Eur. Conf. Comput. Vis. (ECCV)*. pp. 438–452 (2018). https://doi.org/10.1007/978-3-030-01231-1_27
40. Zhu, A.Z., Thakur, D., Ozaslan, T., Pfrommer, B., Kumar, V., Daniilidis, K.: The multivehicle stereo event camera dataset: An event camera dataset for 3D perception. *IEEE Robot. Autom. Lett.* **3**(3), 2032–2039 (Jul 2018). <https://doi.org/10.1109/lra.2018.2800793>
41. Zhu, A.Z., Yuan, L., Chaney, K., Daniilidis, K.: Unsupervised event-based learning of optical flow, depth, and egomotion. In: *IEEE Conf. Comput. Vis. Pattern Recog. (CVPR)*. pp. 989–997 (2019). <https://doi.org/10.1109/CVPR.2019.00108>
42. Zuo, Y., Yang, J., Chen, J., Wang, X., Wang, Y., Kneip, L.: DEVO: Depth-event camera visual odometry in challenging conditions. In: *IEEE Int. Conf. Robot. Autom. (ICRA)*. pp. 2179–2185 (2022). <https://doi.org/10.1109/ICRA46639.2022.9811805>